Numer. Math. Theor. Meth. Appl.
doi: 10.4208/nmtma.2017.y15028

Vol. **10**, No. 3, pp. 656-670
August 2017

Lattice Boltzmann Method for Simulating Phase Separation of Sheared Binary Fluids with Reversible Chemical Reaction

Xiaoyu Wang, Jie Ouyang*, Heng Yang and Jianwei Liu

Department of Applied Mathematics, Northwestern Polytechnical University, Xi'an 710129, China

Received 4 November 2015; Accepted (in revised version) 7 September 2016

Abstract. A lattice Boltzmann method is utilized for governing equations which control phase separation of binary fluids with reversible chemical reaction in presence of a shear flow in this paper. We first present the morphology modeling of sheared binary fluids with reversible chemical reaction. We then validate the model by taking the unsheared binary fluids as an example. It is found that the results fit well with the references. The paper shows structures of the sheared system and gives the detailed analysis for the morphology of sheared binary fluids with reversible chemical reaction. The phase separation of the domain structures with different chemical reaction rates is discussed. Through simulations of the sheared binary fluids, two interesting phenomena are observed, which do not exist in a binary mixture without reversible chemical reaction. One is that the same results appear in both low and high viscosity, and the other is that the domain growth exponent with both low and high viscosities presents wave due to the competition of the viscosity and phase separation. In addition, we find that the finite size effects resulting in the growth exponent decreasing appear faster than that of the unsheared blend at a large time when the size of domains is comparable with the lattice size.

AMS subject classifications: 76D06, 76D07

Key words: Phase separation, reversible chemical reaction, lattice Boltzmann method, sheared binary fluids.

1. Introduction

The effects of a shear flow imposed on the fluid blends have been researched through numerical simulations in the last years. And the investigation indicates that when a fluid blend is quenched from a disordered state to a segregate system, phase separation and morphology of the fluid blends are strongly influenced by different sheared flows [1–5]. In the case of fluid mixtures subjected to a simple shear flow, the structures of domains are always aligned along the flow direction [6–9]. Taking the report written by Lamura and

*Corresponding author. *Email address:* jieouyang@nwpu.edu.cn (J. Ouyang)

 ©2017 Global-Science Press

https://doi.org/10.4208/nmtma.2017.y15028 Published online by Cambridge University Press

Gonnella [8] for example, we can see how the interplay between disordering tendencies of the shear and phase separation leads to a state of dynamic equilibrium where domains are broken up and reformed.

However, among the above reports, the investigated objects are just some simple sheared blends without the chemical reaction. In fact, on one hand, the blends with chemical reaction are of significant importance for industrial engineering and our daily life. On the other hand, Xie et al. [10, 11] show that a shear flow can greatly affect the phase evolution of the multi-component mixtures with the chemical reaction blends by the rheological method. Therefore, it is necessary to investigate the morphology and phase separation of complex sheared mixtures coupling chemical reaction through the numerical simulation. Based on the idea that is from simple to difficult, two-component blends with reversible chemical reaction is researched in this paper.

Moreover, taking existing references into consideration, we find that there is little investigation for phase separation of the sheared binary mixtures with the reversible chemical reaction. It is note that [12, 13] performed early work using numerical method and revealed that many interesting patterns can be obtained in the binary systems with the reversible chemical reaction. So the main purpose of this paper is to see how the shear flow affects the complex binary mixtures with reversible chemical reaction through the numerical simulation.

Based on our target, lattice Boltzmann method (LBM) is utilized in this paper. Lattice Boltzmann method [14–18] originating from the lattice gas automata (LGA) [19–21] has been applied to computational fluid dynamics since 1980s. Compared with traditional macroscopic numerical methods, LBM possesses a lot of advantages including easy-coding, simple handing boundary, natural parallelism and clear physical picture. Furthermore, in the light of its microscopic nature and mesoscopic characteristic, we may truly simulate hydrodynamic effects on phase separation and morphology of complicated fluids. Due to both the above reasons and in absence of research about the shear flow on phase separation with reversible chemical reaction, we utilize LBM to investigate this problem.

2. Model

2.1. Determining the morphologies: governing equations

In this paper, for the sake of simulating the structural evolution of a binary A/B fluids system, we adopt the LBM to model the phase separation in reversible chemical reaction. Here, we characterize our system by one order parameter named φ, which is defined as

$$\varphi = \varphi_A - \varphi_B,$$

where $\varphi_A$and φ_B are the local volume fractions of A and B components.

We chose a free energy function [13, 22]

$$F(\varphi) = \int d\mathbf{r} \left[-\frac{\tau}{2}\varphi^2 + \frac{g}{4}\varphi^4 + \frac{\kappa}{2}(\bigtriangledown\varphi)^2 + \frac{\rho \ln \rho}{3} \right]. \tag{2.1}$$

https://doi.org/10.4208/nmtma.2017.y15028 Published online by Cambridge University Press

Here, the positive constants τ, g and κ are phenomenological parameters. ρ is the density and $\mathbf{r}$ is the position.

The evolution of the order parameter is governed by the following Cahn-Hilliard equation [12]

$$\frac{\partial \varphi}{\partial t} + (\mathbf{u}\nabla)\varphi = M \nabla^2 \frac{\delta F(\varphi)}{\delta \varphi} - (T_1 + T_2)\left(\varphi - \frac{T_2 - T_1}{T_1 + T_2}\right), \tag{2.2}$$

where M is called mobility, T_1 and T_2 are the forward and backward reaction rates, respectively and δ is variational derivative. In the above equation, the hydrodynamic contributions are incorporated through the velocity field $\mathbf{u}$ which is obtained from the Navier-Stokes equation [12]

$$\rho\left[\frac{\partial \mathbf{u}}{\partial t} + (\mathbf{u}\cdot\nabla)\mathbf{u}\right] = -\nabla p + \eta \nabla^2 \mathbf{u} - \varphi \nabla \mu_\varphi. \tag{2.3}$$

Here, η is the kinematic viscosity and p is the pressure. Moreover, we have $\partial_\beta P_{\alpha\beta} = \nabla p + \varphi \nabla \mu_\varphi$ [13], where $P_{\alpha\beta}$ is the thermodynamic pressure tensor. The chemical potential, μ_φ is the functional derivative of the free energy with respect to φ , which is given by $\mu_\varphi = \delta F(\varphi)/\delta\varphi$.

2.2. The model for solving governing equations

To numerically solve Eqs. (2.2) and (2.3), we utilize LBM based on a free-energy function introduced by Swift et al. [22, 23]. Lattice Boltzmann method in this paper is characterized by two distribution functions, f_i and g_i, which are evolved on a simple square lattice with velocity $\mathbf{e}_i$ in two-dimension. The links between the macroscopic physical quantities and the distribution functions are constrained as follows

$$\sum_i f_i^{(eq)} = \rho, \sum_i f_i^{(eq)}\mathbf{e}_i = \rho\mathbf{u}, \sum_i f_i^{(eq)}\mathbf{e}_i\mathbf{e}_i = P_{\alpha\beta}\delta_{\alpha\beta} + \rho\mathbf{u}\mathbf{u}, \tag{2.4a}$$

$$\sum_i g_i^{(eq)} = \varphi, \sum_i g_i^{(eq)}\mathbf{e}_i = \varphi\mathbf{u}, \sum_i g_i^{(eq)}\mathbf{e}_i\mathbf{e}_i = N\mu_\varphi\mathbf{I} + \varphi\mathbf{u}\mathbf{u}, \tag{2.4b}$$

where $f_i^{(eq)}$ and $g_i^{(eq)}$ are equilibrium distribution functions, the choices of which determine the inherent physics in the simulation. $\mathbf{I}$ is the unit matrix. $\delta_{\alpha\beta}$ is the Kronecker delta function, N is related to the mobility M. And specifically, from Eq. (2.1), the pressure tensor [13] can be expressed as

$$P_{\alpha\beta} = \left[\frac{\rho}{3} + \varphi(\tau\varphi + \gamma\varphi^3) - \frac{1}{2}\tau\varphi^2 - \frac{1}{4}\gamma\varphi^4 - \kappa\varphi\nabla^2\varphi - \frac{\kappa}{2}(\nabla\varphi)^2\right]\delta_{\alpha\beta} + \kappa\partial_\alpha\varphi\partial_\beta\varphi. \tag{2.5}$$

We use the D2Q9 (two-dimension and nine-speed) model to recover the governing equations and to simulate the system of the sheared binary blend with reversible chemical reaction. The nine speeds $\mathbf{e}_i$ are $\mathbf{e}_0 = (0,0), \mathbf{e}_1 = (1,0), \mathbf{e}_2 = (0,1), \mathbf{e}_3 = (-1,0), \mathbf{e}_4 = (0,-1), \mathbf{e}_5 = (1,1), \mathbf{e}_6 = (-1,1), \mathbf{e}_7 = (-1,-1), \mathbf{e}_8 = (1,-1)$. The distribution functions f_i

https://doi.org/10.4208/nmtma.2017.y15028 Published online by Cambridge University Press

and g_i, which are based on a single-relaxation-time approximation named LBGK [24–26], are proposed as described below

$$f_i(\mathbf{r}+\mathbf{e}_i\delta t, t+\delta t) = f_i(\mathbf{r},t) - \frac{1}{\tau_f}\left(f_i^{(eq)}(\mathbf{r},t) - f_i(\mathbf{r},t)\right), \tag{2.6a}$$

$$\begin{aligned} g_i(\mathbf{r}+\mathbf{e}_i\delta t, t+\delta t) = {} & g_i(\mathbf{r},t) - \frac{1}{\tau_g}\left(g_i^{(eq)}(\mathbf{r},t) - g_i(\mathbf{r},t)\right) \\ & - \delta t\omega_i\left(1+\lambda\frac{\mathbf{e}_i\cdot\mathbf{u}}{c_s^2}\right)(T_1+T_2)\left(\varphi - \frac{T_2-T_1}{T_1+T_2}\right) \\ & + \frac{\theta\delta t^2}{2}\frac{\partial}{\partial t}\left[(T_1+T_2)\left(\varphi-\frac{T_2-T_1}{T_1+T_2}\right)\right], \end{aligned} \tag{2.6b}$$

where both ω_i and c_s^2 are the parameters linked with the model we chose, in particular $\omega_0 = 4/9, \omega_{1-4} = 1/9, \omega_{5-8} = 1/36$ and $c_s^2 = 1/3$. Here δt is the time step. The parameters λ and θ are related to the macroscopic equation. And, we design the last two term of Eq. (2.6b) following Shi and Guo [27]. We just solve Eqs. (2.2) and (2.3) by iterating the corresponding evolution equations Eqs. (2.6a) and (2.6b) respectively, for a set of distribution functions, instead of directly solving these continuous governing equations. And we set the equilibrium distribution functions, $f_i^{(eq)}$ and $g_i^{(eq)}$, as follows respectively

$$f_0^{(eq)} = A_0 + C_0\mathbf{u}_i\mathbf{u}_i, \tag{2.7a}$$

$$f_I^{(eq)} = A_I + B_I\mathbf{u}_i\mathbf{e}_i + C_I\mathbf{u}_i\mathbf{u}_i + D_I\mathbf{u}_i\mathbf{u}_i\mathbf{e}_i\mathbf{e}_i + G_{I,\alpha\beta}\mathbf{e}_i\mathbf{e}_i, \qquad I = 1\sim 4, \tag{2.7b}$$

$$f_{II}^{(eq)} = A_{II} + B_{II}\mathbf{u}_i\mathbf{e}_i + C_{II}\mathbf{u}_i\mathbf{u}_i + D_{II}\mathbf{u}_i\mathbf{u}_i\mathbf{e}_i\mathbf{e}_i + G_{II,\alpha\beta}\mathbf{e}_i\mathbf{e}_i, \qquad II = 5\sim 8, \tag{2.7c}$$

$$g_0^{(eq)} = H_0 + J_0\mathbf{u}_i\mathbf{u}_i, \tag{2.7d}$$

$$g_I^{(eq)} = H_I + K_I\mathbf{u}_i\mathbf{e}_i + J_I\mathbf{u}_i\mathbf{u}_i + Q_I\mathbf{u}_i\mathbf{u}_i\mathbf{e}_i\mathbf{e}_i, \qquad I = 1\sim 4, \tag{2.7e}$$

$$g_{II}^{(eq)} = H_{II} + J_{II}\mathbf{u}_i\mathbf{e}_i + K_{II}\mathbf{u}_i\mathbf{u}_i + Q_{II}\mathbf{u}_i\mathbf{u}_i\mathbf{e}_i\mathbf{e}_i, \qquad II = 5\sim 8. \tag{2.7f}$$

Substituting Eqs. (2.4) into Eq. (2.7), we have

$$\begin{aligned} &A_0 = \rho - 20A_{II}, && D_I = 4D_{II} = \frac{\rho}{8}, && H_I = 4H_{II} = \frac{N\triangle\mu}{12}, \\ &A_I = 4A_{II} = \frac{P_{xx}+P_{yy}}{24}, && G_{II,xx} = -G_{II,yy} = \frac{P_{xx}-P_{yy}}{16}, && K_I = K_{II} = \frac{\varphi}{12}, \\ &B_I = 4B_{II} = \frac{\rho}{12}, && G_{II,xy} = G_{II,yx} = \frac{P_{xy}}{8}, && J_0 = -\frac{2\varphi}{3}, \\ &C_0 = -\frac{2\rho}{3}, && G_{I,\alpha\beta} = 4G_{II,\alpha\beta}\ (\alpha,\beta = x,y), && J_I = J_{II} = -\frac{\varphi}{24}, \\ &C_I = 4C_{II} = -\frac{\rho}{24}, && H_0 = \varphi - 20H_{II}, && Q_I = Q_{II} = \frac{\varphi}{8}. \end{aligned}$$

https://doi.org/10.4208/nmtma.2017.y15028 Published online by Cambridge University Press

2.3. The Chapman-Enskog expansion for the governing equations

2.3.1. For Navier-Stokes equation

The Eqs. (2.6a) and (2.6b) are equivalent to the governing equations respectively in aspect of mathematics. Therefore, we would recover the corresponding governing equations by the Chapman-Enskog expansion technology [17, 28] based on the proposed Eqs. (2.6a) and (2.6b). For Eq. (2.3), we utilize the Chapman-Enskog in time and space, in particular, as follows:

$$f_i = f_i^{(eq)} + \varepsilon f_i^{(1)} + \varepsilon^2 f_i^{(2)}, \qquad \partial t = \varepsilon \partial t_1 + \varepsilon^2, \qquad \nabla = \varepsilon \nabla_1, \tag{2.8}$$

where, ε is an arbitrarily small positive parameter. Using the former two formulas in Eqs. (2.4a) and (2.8), we have

$$\sum_i f_i^{(n)} = 0, \qquad \sum_i f_i^{(n)} \mathbf{e}_i = 0, \qquad n = 1, 2, \cdots.$$

Applying Taylor expansion to the first term of Eq. (2.6a) in both time and space gives:

$$\delta t(\partial t + \mathbf{e}_i \cdot \nabla) f_i + \frac{\delta t^2}{2}(\delta t + \mathbf{e}_i \cdot \nabla)^2 f_i + \frac{1}{\tau_f}\left(f_i - f_i^{(eq)}\right) + \mathcal{O}(\delta t^3) = 0. \tag{2.9}$$

Substituting Eq. (2.8) into Eq. (2.9) and comparing the terms of ε and ε^2 respectively, we obtain the following equations:

$$\varepsilon: \left(\frac{\partial}{\partial t_1} + \mathbf{e}_i \cdot \nabla\right) f_i^{(eq)} + \frac{1}{\tau_f \delta t} f_i^{(1)} = 0, \tag{2.10a}$$

$$\varepsilon^2: \frac{\partial f_i^{(eq)}}{\partial t_2} + \left(\frac{\partial}{\partial t_1} + \mathbf{e}_i \cdot \nabla\right) f_i^{(1)} + \frac{\delta t}{2}\left(\frac{\partial}{\partial t_1} + \mathbf{e}_i \cdot \nabla\right)^2 f_i^{(eq)} + \frac{1}{\tau_f \delta t} f_i^{(2)} = 0. \tag{2.10b}$$

Applying Eq. (2.10a) to Eq. (2.10b) and simplifying the resulting equation yield

$$\varepsilon^2: \frac{\partial f_i^{(eq)}}{\partial t_2} + \left(\frac{\partial}{\partial t_1} + \mathbf{e}_i \cdot \nabla\right)\left(1 - \frac{1}{2\tau_f}\right) f_i^{(1)} + \frac{1}{\tau_f \delta t} f_i^{(2)} = 0. \tag{2.11}$$

Here, summing Eq. (2.10a) over i and applying the first-velocity moment to Eq. (2.10a), we can get the following macroscopic equations on t_1 scale:

$$\frac{\partial \rho}{\partial t_1} + \nabla_1 \cdot (\rho \mathbf{u}) = 0, \tag{2.12a}$$

$$\frac{\partial (\rho \mathbf{u})}{\partial t_1} + \nabla_1 \cdot (\rho \mathbf{u}\mathbf{u}) = -\frac{\partial P_{\alpha\beta}}{\partial r_1}. \tag{2.12b}$$

In the same way, there are two macroscopic equations on t_2 scale when considering Eq. (2.11). They are

$$\frac{\partial \rho}{\partial t_2} = 0, \qquad \frac{\partial (\rho \mathbf{u})}{\partial t_2} + \nabla_1 \left(1 - \frac{1}{2\tau_f}\right) \sum_i f_i^{(1)} \mathbf{e}_i \mathbf{e}_i = 0. \tag{2.13}$$

https://doi.org/10.4208/nmtma.2017.y15028 Published online by Cambridge University Press

Fortunately, according to Eq. (2.8), the second equation of Eq. (2.13) can be finished for the following form

$$\frac{\partial(\rho\mathbf{u})}{\partial t_2}+\nabla_1\cdot\eta\rho\left(\nabla_1\mathbf{u}+(\nabla_1\mathbf{u})^T\right)=0, \tag{2.14}$$

where

$$\eta=c_s^2(\tau_f-\frac{1}{2})\delta t$$

and due to both the binary fluids' local viscosity's uniform at the spatial positions and the incompressible condition, the second term in Eq. (2.14) becomes the following form

$$\nabla_1\cdot\eta\rho\left(\nabla_1\mathbf{u}+(\nabla_1\mathbf{u})^2\right)=\eta\rho\,\nabla_1^2\,\mathbf{u}.$$

Hence, we finally recover the Navier-Stokes Eq. (2.3) from Eqs. (2.12b) and (2.14) corresponding to the LBGK model.

2.3.2. For Cahn-Hilliard equation

In fact, we would also recover the corresponding governing equation by the Chapman-Enskog expansion technology [17, 28] based on the proposed Eq. (2.6b). For simplicity, we set

$$J=-(T_1+T_2)\left(\varphi-\frac{T_2-T_1}{T_1+T_2}\right), \tag{2.15a}$$

$$J_i=\omega_i J\left(1+\lambda\frac{\mathbf{e}_i\cdot\mathbf{u}}{c_s^2}\right). \tag{2.15b}$$

Then, we have

$$\sum_i J_i=J,\qquad \sum_i\mathbf{e}_iJ_i=\lambda\mathbf{u}J.$$

In order to derive the Cahn-Hilliard Eq. (2.2), we utilize the Chapman-Enskog, in particular, as follows:

$$J=\varepsilon J^{(1)},\qquad g_i=g_i^{(eq)}+\varepsilon g_i^{(1)}+\varepsilon^2 g_i^{(2)}. \tag{2.16}$$

According to Eqs. (2.15a)∼(2.16), then we can get

$$\sum_i J_i^{(1)}=J^{(1)},\quad \sum_i\mathbf{e}_iJ_i^{(1)}=\lambda\mathbf{u}J^{(1)},\quad \sum_i g_i^{(k)}=0\ \ (k\geq 1) \tag{2.17}$$

where

$$J_i^{(1)}=\omega_i J^{(1)}\left(1+\lambda\frac{\mathbf{e}_i\cdot\mathbf{u}}{c_s^2}\right).$$

Applying Taylor expansion to the left first term of Eq. (2.6b) and omitting the high-order terms, we can obtain:

$$\delta t(\partial t+\mathbf{e}_i\nabla)g_i+\frac{\delta t^2}{2}(\partial t+\mathbf{e}_i\nabla)^2g_i+\frac{1}{\tau_g}(g_i-g_i^{(eq)})-J_i-\frac{\theta\delta t}{2}\frac{\partial J_i}{\partial t}=0. \tag{2.18}$$

https://doi.org/10.4208/nmtma.2017.y15028 Published online by Cambridge University Press

Substituting Eqs. (2.8) and (2.16) into Eq. (2.18) and comparing the terms of ε and ε^2 respectively, we obtain the following equations are given very naturally:

$$\varepsilon: \left(\frac{\partial}{\partial t_1}+\mathbf{e}_i\cdot\nabla\right)g_i^{(eq)}+\frac{1}{\tau_g\delta t}g_i^{(1)}-J_i^{(1)}=0, \tag{2.19a}$$

$$\varepsilon^2: \frac{\partial g_i^{(eq)}}{\partial t_2}+\left(\frac{\partial}{\partial t_1}+\mathbf{e}_i\cdot\nabla\right)g_i^{(1)}+\frac{\delta t}{2}\left(\frac{\partial}{\partial t}+\mathbf{e}_i\cdot\nabla\right)^2 g_i^{(eq)} + \frac{1}{\tau_g\delta t}g_i^{(2)}-\frac{\theta\delta t}{2}\frac{\partial J_i^{(1)}}{\partial t_1}=0. \tag{2.19b}$$

Applying Eq. (2.19a) to Eq. (2.19b) and simplifying the resulting equation yield

$$\varepsilon^2: \frac{\partial g_i^{(eq)}}{\partial t_2}+\left(\frac{\partial}{\partial t_1}+\mathbf{e}_i\cdot\nabla\right)\left(1-\frac{1}{2\tau_g}\right)g_i^{(1)} + \frac{1}{\tau_g\delta t}g_i^{(2)}-\frac{\delta t}{2}\mathbf{e}_i\cdot\nabla J_i^{(2)}-\frac{\theta-1}{2}\delta t\frac{\partial J_i^{(1)}}{\partial t_1}=0. \tag{2.20}$$

Here, summing Eqs. (2.19a) and (2.20) over i respectively, we can get the following macroscopic equations:

$$\frac{\partial\varphi}{\partial t_1}+\nabla_1\cdot(\varphi\mathbf{u})=J^{(1)}, \tag{2.21a}$$

$$\frac{\partial\varphi}{\partial t_2}+\nabla_1\cdot\left(1-\frac{1}{2\tau_g}\right)\sum_i g_i^{(1)}\mathbf{e}_i-\frac{\delta t}{2}\nabla\cdot(\lambda\mathbf{u}J^{(1)})-\frac{\theta-1}{2}\delta t\frac{\partial J^{(1)}}{\partial t_1}=0. \tag{2.21b}$$

Based on Eqs. (2.4b), (2.16), (2.19a) and (2.21a), we can induce the following formulation

$$\begin{aligned}\sum_i g^{(i)}\mathbf{e}_i &= -\tau_g\delta t\sum_i\left[\left(\frac{\partial}{\partial t_1}+\mathbf{e}_i\cdot\nabla\right)g_i^{(eq)}-J^{(i)}\right]\mathbf{e}_i\\ &=-\tau_g\delta t\left[\mathbf{u}\frac{\partial\varphi}{\partial t_1}+\nabla\cdot(N\mu_\varphi\mathbf{I}+\varphi\mathbf{u}\mathbf{u})-\lambda J^{(1)}\mathbf{u}\right]\\ &=-\tau_g\delta t\mathbf{u}\left[\frac{\partial\varphi}{\partial t_1}+\nabla\cdot(\varphi\mathbf{u})-J^{(1)}\right]-\tau_g\delta t\left[(1-\lambda)J^{(1)}\mathbf{u}+\nabla N\mu_\varphi\right]\\ &=-\tau_g\delta t\left[(1-\lambda)J^{(1)}\mathbf{u}+N\nabla_1\mu_\varphi\right].\end{aligned} \tag{2.22}$$

Substituting Eq. (2.22) into Eq. (2.21b) and combining Eq. (2.21a), then we have

$$\begin{aligned}&\frac{\partial\varphi}{\partial t}+(\mathbf{u}\cdot\nabla)\varphi\\ &=\left[N(\tau_g-\frac{1}{2})\delta t\right]\nabla^2\mu+J-\delta t\nabla\cdot\left[(\tau_g\lambda-(\tau_g-\frac{1}{2}))J\mathbf{u}\right]-\frac{\theta-1}{2}\delta t\frac{\partial J}{\partial t}.\end{aligned} \tag{2.23}$$

Obviously, the mobility M is set as $M=N(\tau_g-\frac{1}{2})\delta t$. If the parameters λ and θ are chosen respectively as $\lambda=(\tau_g-\frac{1}{2})/\tau_g$ and $\theta=1$, we can get Eq. (2.2) corresponding to the LBGK model.

https://doi.org/10.4208/nmtma.2017.y15028 Published online by Cambridge University Press

2.4. Shear boundary conditions

In the paper, we simulate shear boundary conditions [29] for a shear in the x direction and impose periodic boundary conditions on y direction. The boundary is designed conforming to the above description based on the idea of the nonequilibrium bounce-back scheme proposed by Zou and He [30] and the equilibrium scheme given by Lamura and Gonnella [8]. The computation field is assumed as $x = 0,1,\cdots,nx$, $y = 0,1,\cdots,ny$. And then we give the same velocity v_0 except the reverse direction on the top and bottom boundary, which is the same as a shear flow imposed on the system. In particular, taking the bottom boundary for example, it is obvious that the distributions f_2, f_5, f_6 and density ρ are unknown and that the velocity v_0 is known. Due to conservation of mass and momentum referred to Eq. (2.4(a)), we can get the following equations

$$f_6 + f_2 + f_5 = \rho - f_0 - f_1 - f_3 - f_4 - f_7 - f_8, \tag{2.24a}$$
$$\rho(-v_0) = f_1 - f_3 + f_5 - f_6 - f_7 + f_8, \tag{2.24b}$$
$$f_2 - f_4 + f_5 + f_6 - f_7 - f_8 = 0. \tag{2.24c}$$

Four unknown variables and three equations require us to add another equation for the sake of closed equations. Adopting bounce-back scheme in y direction, that is the equation

$$f_2 = f_4. \tag{2.25}$$

Using Eq. (2.24) and Eq. (2.25), the unknown variables proposed above are presented as follows,

$$\rho = f_0 + f_1 + f_3 + 2(f_4 + f_7 + f_8), \qquad f_2 = f_4,$$
$$f_5 = f_7 - \frac{f_1 - f_3}{2} - \frac{\rho v_0}{2}, \qquad f_6 = f_8 + \frac{f_1 - f_3}{2} + \frac{\rho v_0}{2}.$$

A fluid in the lattice (x, ny) of the top boundary will enter the lattice $(x + v_0 t, 0)$ of the bottom boundary when streaming. Because $v_0 t$ may not be an integer, we need perform a linear interpolation [6, 30] to solve this problem. The scheme in detail is presented like that

$$f_i(x,0) = [1 - H(v_0 t)] f_i(x + I(v_0 t), ny) + H(v_0 t) f_i(x + I(v_0 t) + 1, ny),$$
$$f_i(x,ny) = [1 - H(v_0 t)] f_i(x - I(v_0 t), 0) + H(v_0 t) f_i(x - I(v_0 t) - 1, 0).$$

Here, $I(v_0 t)$ is the largest integer and $H(v_0 t) = v_0 t - I(v_0 t)$.

3. Results and discussions

To validate the model in this paper, phase separation of unsheared binary fluids with reversible chemical reaction is simulated in the first place, which is compared with the literatures [12, 13]. In this example, the lattice size is assumed as 256×256. The density ρ is set 1.0, and the initial velocity $v_0 = 0$. The parameters τ, γ and κ are -0.01, 0.01

https://doi.org/10.4208/nmtma.2017.y15028 Published online by Cambridge University Press

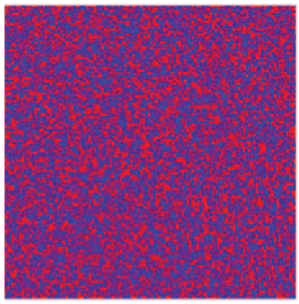
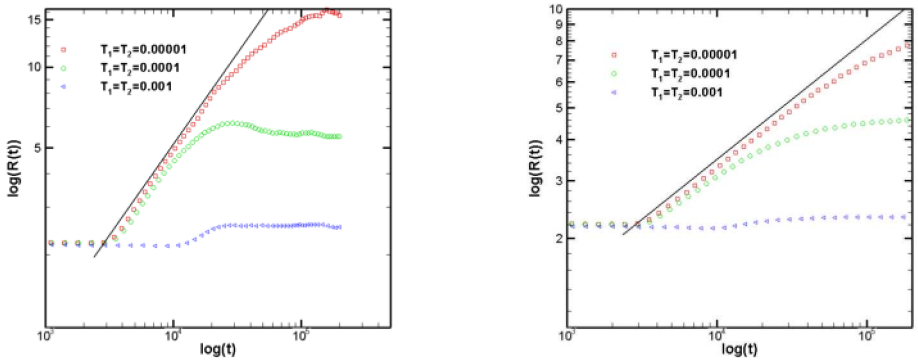


Figure 1: The initial state of the domain structure.

and 0.01, respectively. We choose the relaxation time τ_f through the viscosity η based on $\eta = c_s^2(\tau_f - \frac{1}{2})\delta t$ when coding with $c_s^2 = 1/3, \delta t = 1.0$. Analogously, when mobility M is set to 1.0, then the relaxation time τ_g is given with 1.0. The forward and backward reaction rates are equal. The composition ratio of the A:B (namely $\varphi_A : \varphi_B$) fluids is 1:1, that is to say that the initial theoretical order parameter φ_{ini} is zero. However, for the evolution of the mixtures, we give a little disturbance to the system when coding with $\varphi = \varphi_{ini} \pm 0.01$ through the random function. And in the first, the initial state of all the simulations is shown in Fig. 1, where, the red color represents one component, and the blue stands for the other.

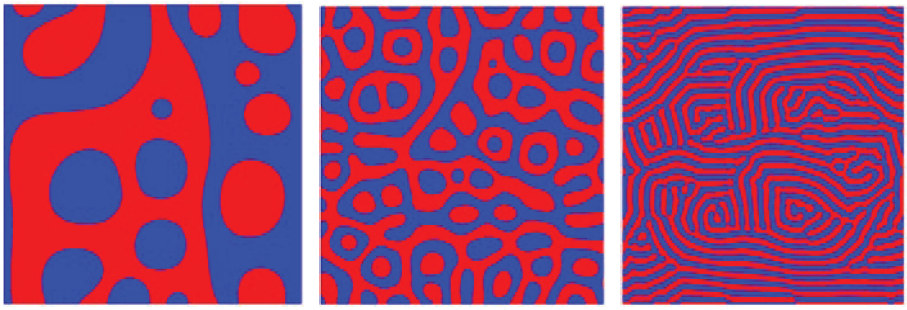
The length-scale properties of domain growth are show in Fig. 2. And the measure of the length-scale property is defined as $R(t) = L_x \cdot L_y / L_I$, here L_x and L_y being the lattice size along the x direction and y direction, respectively. L_I denotes the number of the lattice sites **r** such that $\varphi(\mathbf{r})\varphi(\mathbf{r'}) < 0$, with **r** and **r'** being the nearest neighbor lattice points. For low chemical reaction rate, the domain growth exponent of the late stage with high viscosity is close to $1/3$. And in the case of low viscosity the domain growth exponent seems to be $2/3$. What's more, the domain growth exponent decreases due to the inhibition of domain growth resulting from the competition of chemical reaction and



(a) $\eta = 1$ (b) $\eta = 100$

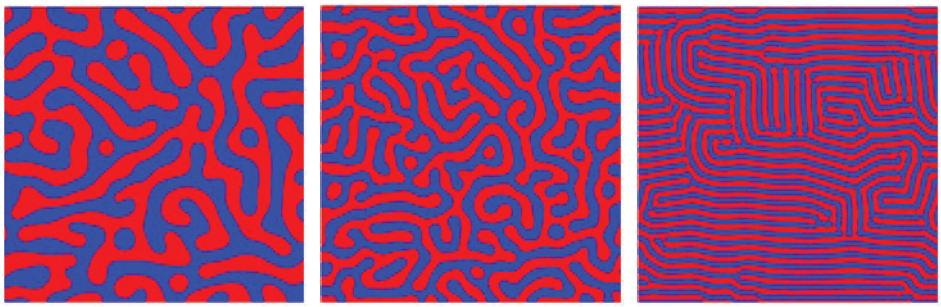
Figure 2: Log-log plot of the scaling form $R(t) \propto t^{\alpha}$ at different chemical reaction rates($v_0 = 0$).

https://doi.org/10.4208/nmtma.2017.y15028 Published online by Cambridge University Press



(a) $T_1 = T_2 = 0.00001$ (b) $T_1 = T_2 = 0.0001$ (c) $T_1 = T_2 = 0.001$

Figure 3: The phase separation of the domain structure with different chemical reaction rates in absence of shear flow ($\eta = 1, v_0 = 0$).



(a) $T_1 = T_2 = 0.00001$ (b) $T_1 = T_2 = 0.0001$ (c) $T_1 = T_2 = 0.001$

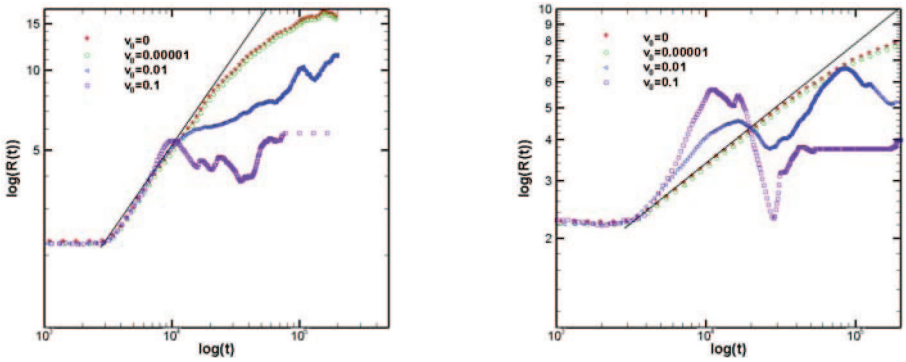
Figure 4: The phase separation of the domain structure with different chemical reaction rates in absence of shear flow ($\eta = 100, v_0 = 0$).

phase separation. Furthermore, the results fit well with the references [12,13,31]. And in next, both the velocity and structures of domains are presented and discussed.

Based on the principle of momentum conversation, the final velocity of the blend should be equal to 0 when the initial velocity is set 0. However, checking the velocity of the system, we find the final velocity of the system isn't absolutely zero. The phenomenon is relate to the spurious current which exists in LBM. Fortunately, the numerical outcomes of the velocity is almost proportional to 0.0001 (tend to 0), even to 0.00001. So the result of LBM we used can be accepted.

Fig. 3 presents the ultimate results of the unsheared fluids with the same viscosity $\eta = 1$ and different chemical reaction rates, which is evolving from Fig. 1. And Fig. 4 shows us other outcomes under the similar condition with $\eta = 100$. From Figs. 3 and 4, we can see that the structure has great changes with the preset conditions and the reversible chemical reaction effects are very important. In particular, the hydrodynamic plays a role in the system with the viscosity $\eta = 1$. We can find that the spontaneous double phase separation (many rain drops form) proposed by Tanaka [31] eclipses with increasing chemical reaction rates. The chemical rate is equal to 0.0001, the phenomenon of double phase separation appears more than others. And, when the chemical reaction

https://doi.org/10.4208/nmtma.2017.y15028 Published online by Cambridge University Press



(a) $\eta = 1$ (b) $\eta = 100$

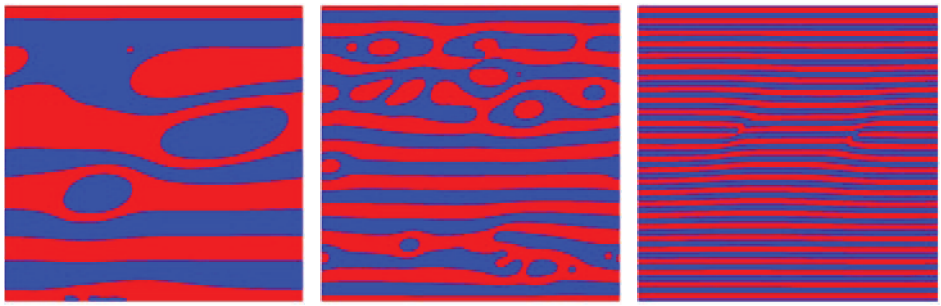
Figure 5: Log-log plot of the scaling form $R(t) \propto t^{\alpha}$ at different shear velocities($T_1 = T_2 = 0.00001$).

rate goes up to 0.001, the lamellar structure is observed with a few of screw morphologies. However, when the viscosity η is equal to 100, instead of double phase separation, the continuous roll rod-like with a network is seen in the Fig. 4. And when the chemical reaction rate $T_1 = T_2 = 0.001$, only the lamellar structures appear in the whole field as shown in Fig. 4(c), which is different from the viscosity $\eta = 1$ compared with the Fig. 3(c). All the results fit well with the literatures. Thereafter, we have faith in the next research on in presence of a shear flow.

In Fig. 5, we give the scaling form $R(t)$ to measure length-scale property at the different velocities with the same chemical reaction $T_1 = T_2 = 0.00001$. The domain growth exponent of the late stage is tending to being equal to $2/3$ with the low viscosity. And in the case for high viscosity the constant decreases to $1/3$. To our knowledge, the results conform to the law of phase separation of binary fluids [6]. In the meanwhile, we find when the velocity v_0 is 0.1, the domain growth exponent of the last stage of the fluids with both low and high viscosities presents wave from Figs. 5(a) and 5(b). The wave fluctuates frequently under the low viscosity, but the amplitude is relatively small. On the contrary, $R(t)$ of the system with high viscosity is just opposite. After a rather long transition, moreover, with the increasing shear velocity, we can find the domain growth exponent quickly decrease to 0, because of the inhibition of domain growth and due to the finite size effects appearing faster than that of the unsheared blend after the same time when the size of domains can be comparable with the lattice size. It implies that the shear flow promotes the evolution of the system's structure and the competition of the last stage just exists in between the viscosity and phase separation.

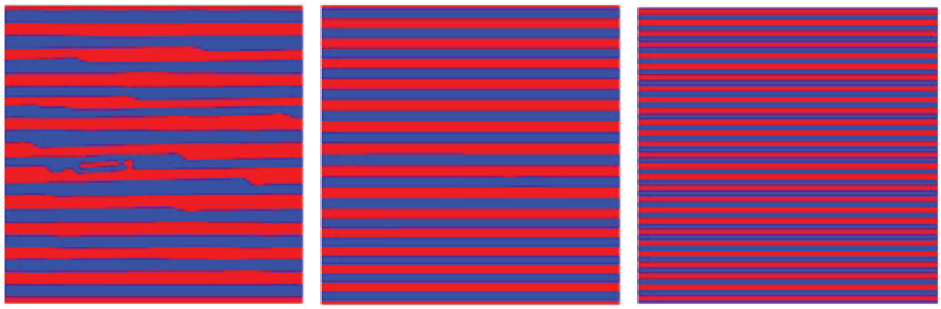
Figs. 6 and 7 show us the final phases of the sheared mixture with the same viscosity and different chemical reaction rates, respectively. We can see that the shear flow has an effect on the morphology of phase separation greatly. Many interesting patterns vary a lot. The all phases heavily tend to the ribbons toward the shear direction with the increasing chemical reaction rates. This phenomenon intrigues us to think that there seems to have a competition among reversible chemical reaction, shear flow and phase separation. The reversible chemical reaction and the shear flow lead to the blend, while the phase separation

https://doi.org/10.4208/nmtma.2017.y15028 Published online by Cambridge University Press



(a) $T_1 = T_2 = 0.00001$ (b) $T_1 = T_2 = 0.0001$ (c) $T_1 = T_2 = 0.001$

Figure 6: The phase separation of the domain structure with different chemical reaction rates in presence of shear flow ($\eta = 1, v_0 = 0.01$).



(a) $T_1 = T_2 = 0.00001$ (b) $T_1 = T_2 = 0.0001$ (c) $T_1 = T_2 = 0.001$

Figure 7: The phase separation of the domain structure with different chemical reaction rates in absence of shear flow ($\eta = 100, v_0 = 0.01$).

takes the components apart. And, the shear flow always suppresses the phase separation.

Taking the low viscosity into account, in Fig. 6, phase separation is smoothly stretched apart in presence of the shear flow, when the viscosity is low ($\eta = 1$) and the chemical reaction rates are low (except $T_1 = T_2 = 0.001$). In addition, a very little like double phase separation is seen in Fig. 6(b). Since hydrodynamics dominate the absolute function, the competition becomes weak leading to the smooth patterns. In spite of the shear flow's effect, we can still infer the pattern of the phase separation of the binary fluids in absence of the shear flow. Comparing Figs. 6(a) and 6(b) referring to the same part in Figs. 3 and 4, a little double phase separation still exists. That is to say, the chemical reaction can compete with the shear function, when the reversible reaction rate is appropriate ($T_1 = T_2 = 0.0001$) with the low viscosity. It implies that if we want to obtain some structures we need, we should have a few of simulation tests with different parameters at first.

With the high viscosity ($\eta = 100$) and a shear flow imposed on the system as shown in Fig. 7, the structures of phase separation are easily aligned with the lower reversible chemical reaction. The property of the high viscosity competes with the shear flow strongly, which makes the relative resistance force strong, so we can see the stripes with raw edges despite the rather lower reversible chemical reaction ($T_1 = T_2 = 0.00001$, tending to

https://doi.org/10.4208/nmtma.2017.y15028 Published online by Cambridge University Press

zero but not equating zero). When the rate increases to 0.0001, the whole area seems to be the wide ribbons. This phenomenon shows that, when the viscosity $\eta = 100$, both the relatively high reversible chemical reaction rate and the shear flow control the morphology of the binary blend in common.

It interests us that the same results and the periodic ribbons appear in Figs. 6(c) and 7(c) when the reversible chemical reaction rate is high ($T_1 = T_2 = 0.001$). This strange phenomenon doesn't exist in a binary mixture without reversible chemical reaction compared with the research made by Wagner and Yeomans [6]. We can say the viscosity is no longer the main reason of the structure of the binary fluids with the reversible chemical reaction. Both the reversible chemical reaction and the shear flow leading to blend play important roles in the morphology of the blend. So, if we need the Fig. 6(c) or Fig. 7(c), we just improve the velocity of the shear flow to avoid increasing the high viscosity bringing us some trouble.

4. Conclusions

In this paper, the model coupling the Eqs. (2.2) and (2.3) based on LBM method is used for simulating phase separation of sheared binary fluids with reversible chemical reaction. The results show that this model can be applied to investigate the problem we consider. Through the results and discussions, we find that when the shear flow is imposed on the fluid, the structures of phase separation tend to the shear direction. In particular, phase separation is smoothly stretched apart and a very little like double phase separation is observed when the fluid viscosity is low. However, the structures of phase separation are easily aligned with the raw edges when the fluid viscosity is high.

Besides, it is interesting that the periodic ribbons are observed in the sheared blend with the same relatively high reversible chemical reaction rate but different viscosities, which doesn't exist in a binary mixture without reversible chemical reaction. We can take a conclusion that the viscosity isn't the cause of the morphology of the system in presence of the shear flow with the relatively high reversible chemical reaction. In the meanwhile, we find that the scaling form $R(t)$ of the fluids with the chemical reaction $T_1 = T_2 = 0.00001$ presents wave, when the velocity v_0 is 0.1. Moreover, the domain growth exponent of the late stage is tending to being a constant with the decreasing velocity and the results conform to the law of phase separation of binary fluids.

Finally, when validating the model in this paper, we find there is the spurious current which exists in LBM. The numerical outcomes of the velocity is almost proportional to 0.0001. However, due to the principle of momentum conversation, the final velocity of the blend should be absolutely equal to 0. So the shortcoming has more or less impacted on the results of phase separation of the sheared binary mixtures. We will further improve the LBM in this paper in follow-up work to decrease the effect of the spurious current.

Acknowledgments Project was supported by the National Basic Research Program of China (No. 2012CB025903), the National Natural Science Foundation of China (No. 91434 201 and No. 11402210).

https://doi.org/10.4208/nmtma.2017.y15028 Published online by Cambridge University Press

References

[1] T. Isojima, H. Kato, and K. Hamano, *Effective viscosities of a phase-separating binary mixture imposed to shear*, Physics Letters A, 240(4) (1998), pp. 271–275.

[2] X. B. Chen, L. S. Niu and H. J. Shi, *Modeling the phase separation in binary lipid membrane under externally imposed oscillatory shear flow*, Colloid. Surface. B., 65(2) (2008), pp. 203–212.

[3] R. S. Qin, *Thermodynamic properties of phase separation in shear flow*, Computers & Fluids, 117(2015), pp. 11–16.

[4] A. G. Xu, G. Gonnella, and A. Lamura, *Phase-separating binary fluids under oscillatory shear*, Phys. Rev. E, 67(5) (2003), 056105.

[5] J. Cui, Z. W. Ma, W. Li, and W. Jiang, *Self-assembly of diblock copolymers under shear flow: A simulation study by combining the self-consistent field and lattice boltzmann method*, Chem. Phys., 386(1) (2011), pp. 81–87.

[6] A. J. Wagner and J. M. Yeomans, *Phase separation under shear in two-dimensional binary fluids*, Phys. Rev. E, 59(4) (1999), pp. 4366–4373.

[7] X. B. Chen, L. S. Niu, and H. J. Shi, *Numerical simulation of the phase separation in binary lipid membrane under the effect of stationary shear flow*, Biophys. chem., 135(1) (2008), pp. 84–94.

[8] A. Lamura and G. Gonnella, *Lattice boltzmann simulations of segregating binary fluid mixtures in shear flow*, Physica A, 294(3) (2001), pp. 295–312.

[9] Y. C. Li, R. P. Shi, C. P. Wang, X. J. Liu, and Y. Z. Wang, *Phase field study on the effect of shear flow on polymer phase separation*, Procedia Engineering, 27(2012), pp. 1502–1507.

[10] F. Xie, C. X. Zhou, W. Yu, and J. Y. Liu, *Heterogeneous polymeric reaction under shear flow*, J. appl. polym. sci., 109(4) (2008), pp. 2737–2745.

[11] F. Xie, C. X. Zhou, and W. Yu, *Effects of small-amplitude oscillatory shear on polymeric reaction*, Polym. Composite., 29(1) (2008), pp. 72–76.

[12] Y. L. Huo, X. L. Jiang, H. D. Zhang, and Y. L. Yang, *Hydrodynamic effects on phase separation of binary mixtures with reversible chemical reaction*, J. Chem. Phys., 118(21) (2003), pp. 9830–9837.

[13] K. Furtado and J. M. Yeomans, *Lattice boltzmann simulations of phase separation in chemically reactive binary fluids*, Phys. Rev. E, 73(6) (2006), 066124.

[14] Y. Y. Yan, Y. Q. Zu, and B. Dong, *LBM, a useful tool for mesoscale modelling of single-phase and multiphase flow*, Appl. Therm. Eng., 31(5) (2001), pp. 649–655.

[15] S. Leclaire, N. Pellerin, M. Reggio, and J. Yves Trépanier, *Multiphase flow modeling of spinodal decomposition based on the cascaded lattice Boltzmann method*, Physica A, 406(2014), pp. 307–319.

[16] H. B. Huang, J. J. Huang, and X. Y. Lu, *A mass-conserving axisymmetric multiphase lattice boltzmann method and its application in simulation of bubble rising*, J. Comput. Phys., 269 (2014), pp. 386–402.

[17] J. F. Zhang, L. M. Wang, and J. Ouyang, *Lattice boltzmann model for the volume-averaged navier-stokes equations*, EPL (Europhysics Letters), 107(2) (2014), 20001.

[18] A. Fakhari and T. H. Lee, *Numerics of the lattice Boltzmann method on nonuniform grids: standard lbm and finite-difference lbm*, Computers & Fluids, 107 (2015), pp. 205–213.

[19] S. Succi, E. Foti, and F. Higuera, *Three-dimensional flows in complex geometries with the lattice Boltzmann method*, EPL (Europhysics Letters), 10(5) (1989), pp. 433.

[20] F. J. Higuera et al, *Boltzmann approach to lattice gas simulations*, EPL (Europhysics Letters), 9(7) (1989), pp. 663.

[21] A. G. Xu, G. Gonnella, and A. Lamura, *Phase separation of incompressible binary fluids with*

https://doi.org/10.4208/nmtma.2017.y15028 Published online by Cambridge University Press

lattice Boltzmann methods, Physica A, 331(1) (2004), pp. 10–22.
[22] M. R. Swift, W. R. Osborn, and J. M. Yeomans, *Lattice Boltzmann simulation of nonideal fluids*, Phys. Rev. Lett., 75(5) (1995), pp. 830.
[23] M. R. Swift, E. Orlandini, W. R. Osborn, and J. M. Yeomans, *Lattice Boltzmann simulations of liquid-gas and binary fluid systems*, Phys. Rev.E, 54(5) (1996), pp. 5041.
[24] S. Y. Chen, H. D. Chen, D. Martnez and W. Matthaeus, *Lattice Boltzmann model for simulation of magnetohydrodynamics*, Phys. Rev. Lett., 67(27) (1991), pp. 3776.
[25] Y. H. Qian, D.Q. d'Humières, and P. Lallemand, *Lattice BGK models for Navier-Stokes equation*, EPL (Europhysics Letters), 17(6) (1992), pp. 479.
[26] Y. H. Qian and S. A. Orszag, *Lattice bgk models for the navier-stokes equation: Nonlinear deviation in compressible regimes*, EPL (Europhysics Letters), 21(3) (1993), pp. 255.
[27] B. C. Shi and Z. L. Guo, *Lattice Boltzmann model for nonlinear convection-diffusion equations*, Phys. Rev. E, 79(1) (2009), 016701.
[28] J. S, J. Ouyang, X. D. Wang, and B. X. Yang, *Lattice Boltzmann method coupled with the oldroyd-b constitutive model for a viscoelastic fluid*, Phys. Rev. E, 88(5) (2013), 053304.
[29] A. J. Wagner and I. Pagonabarraga, *Lees–edwards boundary conditions for lattice boltzmann*, J. stat. phys., 107(1-2) (2002), pp. 521–537.
[30] Q. S. Zou and X. Y. He, *On pressure and velocity boundary conditions for the lattice boltzmann bgk model*, Phys. Fluids, 9(6) (1957), pp. 1591–1598.
[31] H. Tanaka and T. Araki, *Spontaneous double phase separation induced by rapid hydrodynamic coarsening in two-dimensional fluid mixtures*, Phys. Rev. Lett., 81(2) (1989), pp. 389.

https://doi.org/10.4208/nmtma.2017.y15028 Published online by Cambridge University Press